Manuel ROMÁN-LUMBRERAS[1], Guillermo VELASCO-QUESADA[1], Alfonso CONESA-ROCA[1], Ramón BARGALLÓ-PERPIÑÁ[1], Felipe JEREZ[2]
Technical University of Catalonia (1), PREMO Group (2)

Real-Time Parameter Determination in Inductors Submitted to Non-Sinusoidal Currents

Abstract. *This paper presents a procedure for the characterization of inductors when operate under combination of low-frequency sinusoidal current (50 or 60 Hz) and high frequency current, up to 20 kHz, produced in the PWM process. These currents are typical on inductors installed between the power converter output and the electric grid in photovoltaic generation plants. This procedure allows the determination of the inductance value, the value of series and parallel resistance associated with the inductor winding, and then, the power losses corresponding to copper and core.*

Streszczenie. *W artykule analizowano dławik pracujący przy kombinacji prądu sinusoidalnego małej częstotliwości i prądu dużej częstotliwości do 20 kHz wytwarzanego przez układy PWM. Tego typu praca jest typowa gdy dławik jest włączony między przekształtnik a sieć zasilaną a generatorów fotowoltaicznych. (**Określanie w czasie rzeczywistym parametrów dławika dołączonego do prądów niesinusoidalnych**)*

Keywords: Inductor Losses Measurement, Test Equipment, Inductor Model.
Słowa kluczowe: dławik, straty mocy.

Introduction

Any renewable energy system is designed looking for maximum system efficiency at all times, both in build process as in the processing and transfer energy to the electric grid.

In photovoltaic power plants, the whole energy produced flows through one or more static converters, for this reason it is fundamental that these converters present the maximum efficiency as possible. This implies that the losses were minimal, not only in semiconductor components, also in other components such as inductors for coupling the inverter with the electric grid.

For these inductors simultaneously flows the fundamental component of the current, with the grid frequency and in phase with the grid voltage, and current harmonic components originated in the PWM process of the inverter control. For this reason, the design of these inductors is more complex than the design of an inductor that operates only with the fundamental component of current (at 50 Hz or 60 Hz).

The problem is further complicated when the balance between the losses, the accuracy of their inductance value, and the manufacturing cost is looked.

Therefore, the design and construction of a platform for testing these inductors appears as necessary. This platform will serve for testing and control the quality of fabricated inductors, and as a tool in the design and optimization of them.

In this regard, this platform incorporates a system for the determination of main parameters that characterizes the inductors under test. These parameters are: inductance (L), series resistance (RS) and parallel resistance (RP) of the model shown in Fig. 1.

Finally, the values of series and parallel resistance are used for copper and core losses estimation.

Hardware description

A. Equipment for testing inductors

The equipment designed for the test of inductors behaves as an AC/AC converter connected to the grid at both the input and the output. Fig. 2 shows the block diagram of this system, identifying the different elements and how they are interconnected.

The AC/DC converter is a non-controlled three-phase full wave rectifier and the DC/AC converter is based on a three-phase full bridge inverter. This equipment is described in more detail in [1].

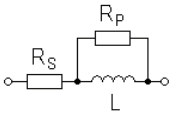

Fig.1. Inductor model considered for parameters estimation

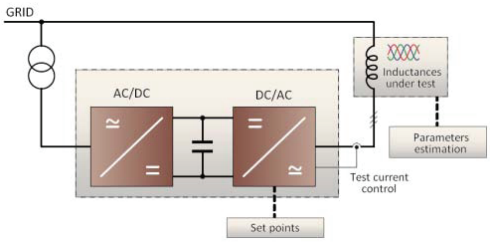

Fig.2. Block diagram of test equipment

B. Equipment for inductor's parameters estimation

The real-time estimation of the inductor's parameters is based on their voltage and current waveforms. For the acquisition of voltage and current on the inductor, a data acquisition (DAQ) card and signal conditioning circuit has been used.

The signal conditioning circuit is based on hall-effect current sensors and low distortion isolated amplifiers. Fig. 3 shows the signal conditioning circuit utilized for one inductor characterization. The designed equipment uses three circuits as this, one per phase.

The used DAQ card is manufactured by National Instruments and it is connected to personal computer (PC) through an USB port.

Finally, the inductor's parameter estimation is realized with a PC using specially programmed application.

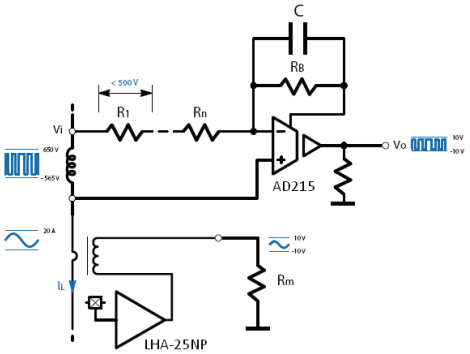

Fig.3. Signal conditioning circuit for voltage/current measurement

Inductor's parameters Estimation

Various methods for inductor's parameters estimation can be found in the specialized literature, [2-5].

The method proposed, and described below, is based on two conditions that often occur in practice:

- The difference between the frequency of the current fundamental component (f_{LF}) and the frequency of the current harmonics due PWM process (f_{HF}) is greater than 10 ($f_{HF} > 10 \cdot f_{LF}$).
- The current peak value due to current harmonics (I_{HF}) is between 10 % and 20 % of the fundamental current (I_{LF}) peak value ($I_{HF} = 0.1 \cdot I_{LF} \div 0.2 \cdot I_{LF}$).

In addition, amorphous magnetic materials and based on Fe-Si are considered. These materials are commonly used in middle and high power applications.

The value of commonly used switching frequencies ($f_{HF} \leq 20$ kHz) and the use of constructive precautions suggests that copper losses are only due to low frequency component of current. On the other hand and as can be deduced from the well known expressions [6-7] by Steinmetz (1) and Bertotti (2), the core losses are strongly dependent with the frequency.

$$P_{core} = K_h \cdot f \cdot B^{\alpha} + K_c \cdot (f \cdot B)^2 \tag{1}$$

$$P_{core} = K_h \cdot f \cdot B^{\alpha} + K_c \cdot (f \cdot B)^2 + K_a \cdot (f \cdot B)^{3/2} \tag{2}$$

Thus, the series resistance (R_S) is associated with copper losses at low frequency, while the parallel resistance (R_P) is associated with core losses at high frequency.

A. Calculation model

For the parameters determination, a calculation model is used in which high frequency (V_{HF}, I_{HF}) and low frequency (V_{LF}, I_{LF}) components of voltage and current on the inductor under test are discriminated using a filter.

In this way, the calculation process is as follows:

$$P_{copper} \cong P_{LF} = \frac{1}{T} \cdot \int_0^T v_{LF}(t) \cdot i_{LF}(t) \cdot dt \tag{3}$$

$$R_S = \frac{P_{LF}}{I_{LF\,rms}^{\,2}} \tag{4}$$

$$P_{core} \cong P_{HF} = \frac{1}{T} \cdot \int_0^T v_{HF}(t) \cdot i_{HF}(t) \cdot dt \tag{5}$$

$$R_P = \frac{V_{HF\,rms}^{\,2}}{P_{core}} \tag{6}$$

The value of L is determined from the ratio of the RMS value of the low frequency voltage at its terminals (V_{LF}) and the low frequency current flowing through it (I_{LF}), according to the following expressions:

$$V_L = RMS\left[v_L(t)\right] = RMS\left[v_{LF}(t) - R_S \cdot i_{LF}(t)\right] \tag{7}$$

$$I_L = RMS\left[i_{LF}(t) - \frac{v_L(t)}{R_P}\right] \tag{8}$$

$$L = \frac{V_L}{I_L \cdot \omega_{LF}} \tag{9}$$

B. Simulation results

To verify the proposed method for parameters estimation, the PSIM simulator has been used, instead of a numeric simulator. This is because LabVIEW is used, as a graphical tool, to program the parameter identification application, and both programs have a similar graphical description of the system to simulate or implement.

The model used for the inductance is shown in Fig. 1, and the values used for its parameters are similar to the values that can be found in a real case.

Fig. 4 shows the circuit used for simulation purposes. It shows the model of the inductor, and sources used to generate a sinusoidal low-frequency current ($f_{LF} = 50$ Hz) with a triangular high-frequency current ($f_{HF} > 10 \cdot f_{LF}$) superimposed. This current is obtained, as can be shown in the figure, using a current source controlled by a voltage source.

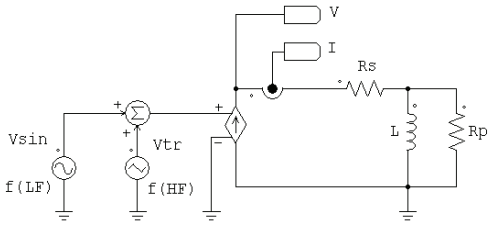

Fig.4. PSIM simulation circuit

Figs. 5, 6 and 7 show the circuits used in the simulation to calculate the values of R_S, R_P and L, according to Eqs. (4), (6) and (9) respectively.

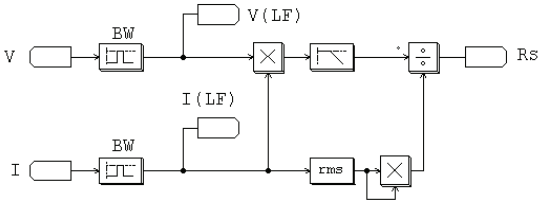

Fig.5. Circuit for R_S estimation

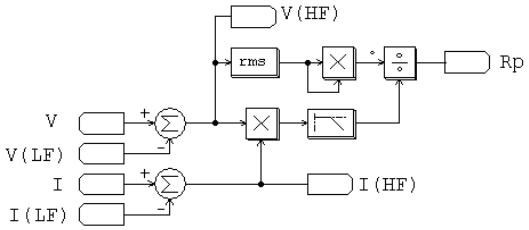

Fig.6. Circuit for R_P estimation

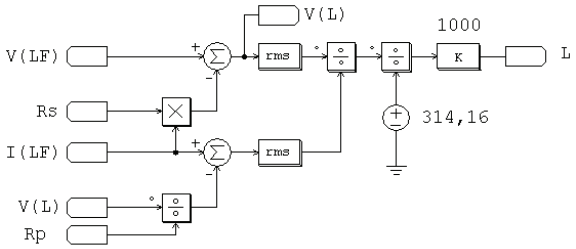

Fig.7. Circuit for L estimation (in mH)

In these circuits, the low-frequency (LF) components of current and voltage are obtained using band-pass filters with the central frequency equal to f_{LF}.

By the other hand, the definite integrals used for power calculations (the average value of current and voltage products) are implemented using second order low-pass filters with cut-off frequency located one decade below the frequencies of the signals of interest.

For simulation purposes a 1.2 mH, 20 A and single-phase inductance is used. These values imply a voltage drop of approximately 3 %, over a network of 230 V / 50 Hz, when the nominal current flows through the inductor.

The current source used imposes a 20 A and 50 Hz sinusoidal current with a 10 A_{PP} (2.88 A_{RMS}) triangular high frequency current superimposed.

The selected values for the other parameters of the inductor are: R_S = 40 mΩ and R_P = 500 Ω.

Fig. 8 shows the voltage and current waveforms on the inductor when the frequency of the high-frequency current component is selected to f_{HF} = 1 kHz.

Table 1 shows the results obtained on the simulation process. These results are obtained from Eqs. (3) and (5) when the current through the inductor has a 20 A and 50 Hz low-frequency sinusoidal component and a 10 A_{PP} high-frequency triangular component. The obtained results for different high-frequency values (switching frequency) are shown.

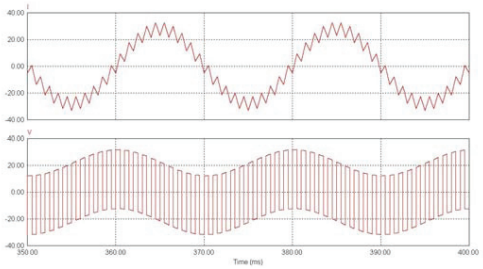

Fig.8. Voltage and current on the inductor for f_{HF} = 1 kHz

Table 1. Eqs. (3) and (5) simulation results

f_{HF}	R_S	R_P	L	P_{copper}	P_{core}	P_{total}
(Hz)	(mΩ)	(Ω)	(mH)	(W)	(W)	(W)
500	40.26	231.16	1.202	15.78	0.62	16.40
1000	40.26	387.02	1.202	15.78	1.47	17.25
2500	40.26	477.43	1.202	15.78	7.36	23.14
5000	40.26	494.05	1.202	15.78	27.81	43.59
10000	40.26	498.46	1.202	15.78	104.95	120.73
20000	40.26	499.30	1.202	15.78	222.86	238.64

These results indicate the following:

- Good results are obtained in the calculation of the series resistance (R_S), the associated losses (P_{copper}) and the inductance value L.
- The determination of parallel resistance (R_P) and the associated losses (P_{core}) are more accurate when the frequency of the high-frequency current component (f_{HF}) is higher.
- The power losses in the wires (copper losses) are not affected by the switching frequency, at least with the current values considered, and power losses in the core grows roughly in line with the quadratic equations (1) and (2) .

C. Experimental results

The experimental data were obtained using the power system and data acquisition system previously described.

The power system used is shown in Fig. 9 and corresponds to the block diagram shown in Fig. 2.

With this equipment, a 1.2 mH / 20 A three-phase inductor, manufactured by PREMO Group, has been tested. This inductor is built using amorphous magnetic material, and it is shown in Fig. 10.

The calculation algorithm used, which is implemented using LabVIEW software, implements the model described in Eqs. (3) and (5).

Fig. 11 shows the values obtained when a switching frequency of 10 kHz and a current about 22 A_{RMS} is used. This figure shows the current and voltage waveforms in one coil of the tested inductor, and the values for R_S, R_P, L and losses estimated by the system implemented.

Fig. 12 shows the waveforms and RMS values of voltages and currents in each phase of the inductor under test. These data also correspond to a switching frequency of 10 kHz and a current about 22 A_{RMS} per phase.

Fig.9. Equipment for inductor tests

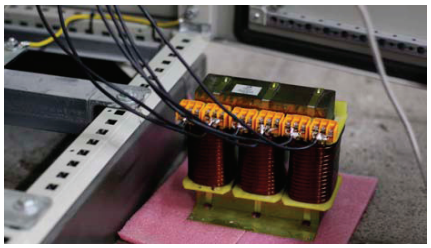

Fig.10. Three-phase inductor under test

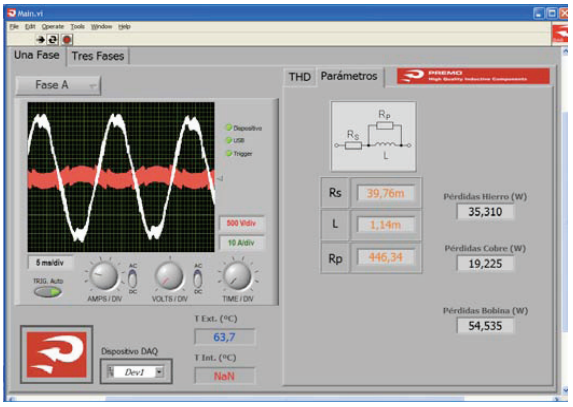

Fig.11. Estimated values for the parameters of one phase of the inductor under test. The current and voltage waveforms on this inductor are also shown

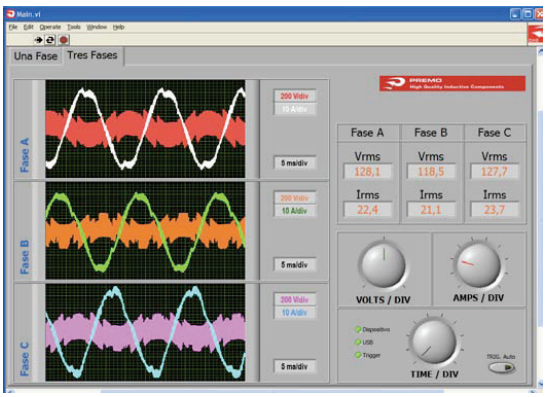

Fig.12. Current and voltage waveforms, and the corresponding RMS, value on the inductor under test

Table 2. 11 A_{RMS} experimental results

f_{HF} (Hz)	R_S (mΩ)	R_P (Ω)	L (mH)	P_{copper} (W)	P_{core} (W)	P_{total} (W)
5000	41.30	473.42	1.15	5.18	37.51	42.69
10000	37.41	468.64	1.16	5.26	35.64	40.90
15000	34.64	474.71	1.15	4.81	34.60	39.41
20000	34.21	441.68	1.20	3.83	35.24	39.07

Table 3. 22 A_{RMS} experimental results

f_{HF} (Hz)	R_S (mΩ)	R_P (Ω)	L (mH)	P_{copper} (W)	P_{core} (W)	P_{total} (W)
5000	41.83	386.95	1.18	21.52	43.00	64.52
10000	39.76	446.34	1.14	19.22	35.31	54.53
15000	40.95	432.35	1.16	20.49	35.61	56.10
20000	41.61	412.52	1.18	17.81	35.92	53.73

Tables 2 and 3 show the results obtained for different values of switching frequency (f_{HF}) and two different RMS values of current through the inductor under test (11 and 22 A_{RMS}).

As it can be seen, both the equivalent resistance values (R_S and R_P) and the inductance value (L) are obtained with variations of less than 10 % below the average value obtained for the same test current. This accuracy is sufficient taking into account the values prescribed in the most common applications of these magnetic components.

On the other hand, it is observed that core power losses (P_{core}) value is practically independent of the RMS value of the used current for performing the test. This result is in consistency with the assumption that the core losses mainly depend on the high-frequency component of the current through the inductor.

At first glance, the fact that the value of R_P and the associated core losses (P_{core}) are practically independent with the frequency of the high-frequency current component, may seem strange. This kind of dependence can be seen in simulation results, shown in Table 1, but not in experimental results shown in Tables 2 and 3.

This behavior occurs because a voltage source power converter (VSC) has been used for performing the tests. On these converters, a change in the switching frequency results in a change in the ripple current and, therefore, in a variation of the magnetic induction (B) for the high-frequency current component. This variation of B is, in theory, inversely proportional to the converter switching frequency. As a result, and accordingly with Eqs. (1) and (2), it is possible to justify that the increase in losses due to the increase of switching frequency, may be compensated by the reduction in B.

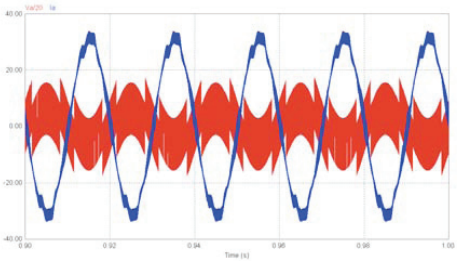

Fig.13. Simulated current and voltage waveforms on the inductor under test obtained using f_{HF} = 10 kHz

Finally, Fig. 13 shows the current and voltage waveforms in one phase of a three-phase inductor. These waveforms are obtained by simulation using the data shown in Table 3 for a 10 kHz switching frequency.

For this simulation, a power system as shown in Fig. 2 is used, and the method based on equations (3) and (5) is applied in order to obtain the current and voltage waveforms.

As can be seen, the obtained waveforms are very similar to the measured waveforms, and shown in Figs. 11 and 12.

Conclusions

This paper presents a procedure for measuring, in real operating conditions, the main parameters of inductors when submitted to currents formed by combination of low and high frequency components. This kind of current is typical in grid connected converters for photovoltaic applications.

The described procedure is based on the acquisition of the voltage and current on the inductance under test, and taking in account the frequency and RMS current values commonly used in the intended applications. This assumption allows us to consider that the low-frequency current component basically generates the copper losses (P_{copper}), while the high-frequency current component basically generates the core losses (P_{core}).

The method described has been experimented. It was applied, for testing in real conditions, in a commercial 1.2 mH inductor. The results obtained are valid and consistent with the results expected.

This work has been developed in collaboration with PREMO Group and was partially funded by the PROFIT program of the Spanish Ministry of Industry and Energy under the project reference: FIT-330100-2006-20.

REFERENCES

[1] R. Pérez, A. Codina, M. Román, A. Conesa and G. Velasco, "Convertidor CA/CA para ensayo de Inductancias con Retorno de Energía a Red", 17º Seminario Anual de Automática, Electrónica Industrial e Instrumentación (SAAEI 10). July 2010. In Spanish.

[2] Perpiña, R.B.; Lumbreras, M.R.; Roca, A.C. and Quesada. G.V., "Real time parameter and models determination in saturated inductors submitted to non-sinusoidal excitations", 13th European Conference onPower Electronics and Applications, 2009 (EPE'09). Sep. 2009.

[3] W. Marshall Leach, Jr., "Loudspeaker Voice-Coil Inductance Losses: Circuit Models, Parameter Estimation, and Effect on Frequency Response", Journal of the Audio Engineering Society, Vol. 50, Nº. 6, June 2002.

[4] Ruinan Chang and Wenjun Zhang, "A comprehensive linearregression- based Procedure for inductor parameter extraction", VLSI Design, Automation and Test, 2009. VLSI-DAT '09. International Symposium on , vol., no., pp.287-290, 28-30 April 2009.

[5] Monteiro, T.C.; Martinz, F.O.; Komatsu, W. and Matakas, L., "A method of transformer parameters determination for power electronics applications", Power Electronics Conference, 2009. COBEP '09. Brazilian , vol., no., pp.1019-1026, 2009.

[6] G. Bertotti, "General properties of power losses in soft ferromagnetic materials," IEEE Trans. Magn., vol. 24, no. 1, pp. 621–630, Jan. 1988.

[7] J. Reinert, A. Brockmeyer R. Donker, "Calculation of Losses in Ferroand Ferrimagnetic Materials Based on the Modified Steinmetz Equation" IEEE Transaction on Ind. Applications, Vol 37, Nº 4, July/August 2001.

Authors: *Prof. M. Román-Lumbreras, College of Industrial Engineering of Barcelona, Technical University of Catalonia (UPC), C. Urgell 187, 08036 - Barcelona (Spain), Manuel.Roman@upc.edu. Prof. G. Velasco-Quesada, College of Industrial Engineering of Barcelona, Technical University of Catalonia (UPC), Guillermo.Velasco@upc.edu. Prof. A. Conesa-Roca, College of Industrial Engineering of Barcelona, Technical University of Catalonia (UPC), Alfonso.Conesa@upc.edu. Prof. R. Bargalló-Perpiña, College of Industrial Engineering of Barcelona, Technical University of Catalonia (UPC), Ramon.Bargallo@upc.edu. Sr. Felipe Jerez, PREMO Group, C. Conchita Supervía 13, 08028 - Barcelona (Spain), Felipe.Jerez@grupopremo.com.*